

Supplementary information and data

The rise of oxygen-driven arsenic cycling ~2.48 Gyr ago

Ernest Chi Fru^{1*}, Andrea Somogyi², Abderrazzak El Albani³, Kadda Medjoubi², Jérémie Aubineau³, Leslie J. Robbins⁴, Stefan V. Lalonde⁵, Kurt O. Konhauser⁴

¹College of Physical and Engineering Sciences, School of Earth and Ocean Sciences, Geobiology Centre, Cardiff University, Cardiff CF10 3AT, Wales, UK.

²Nanoscopium beamline Synchrotron Soleil, L'Orme des Merisiers Saint-Aubin-BP 48, 91192 GIF-sur-YVETTE CEDEX, France.

³Université de Poitiers UMR 7285-CNRS, Institut de Chimie des Milieux et Matériaux de Poitiers - 5, rue Albert Turpin (Bât B35) 86073 Poitiers cedex, France.

⁴Department of Earth and Atmospheric Sciences University of Alberta Edmonton, Alberta, T6G 2E3 Canada.

⁵CNRS-UMR6538 Laboratoire Géosciences Océan (LGO), European Institute for Marine Studies, Université de Bretagne Occidentale, 29280 Plouzané, France.

SUPPLEMENTARY DATA

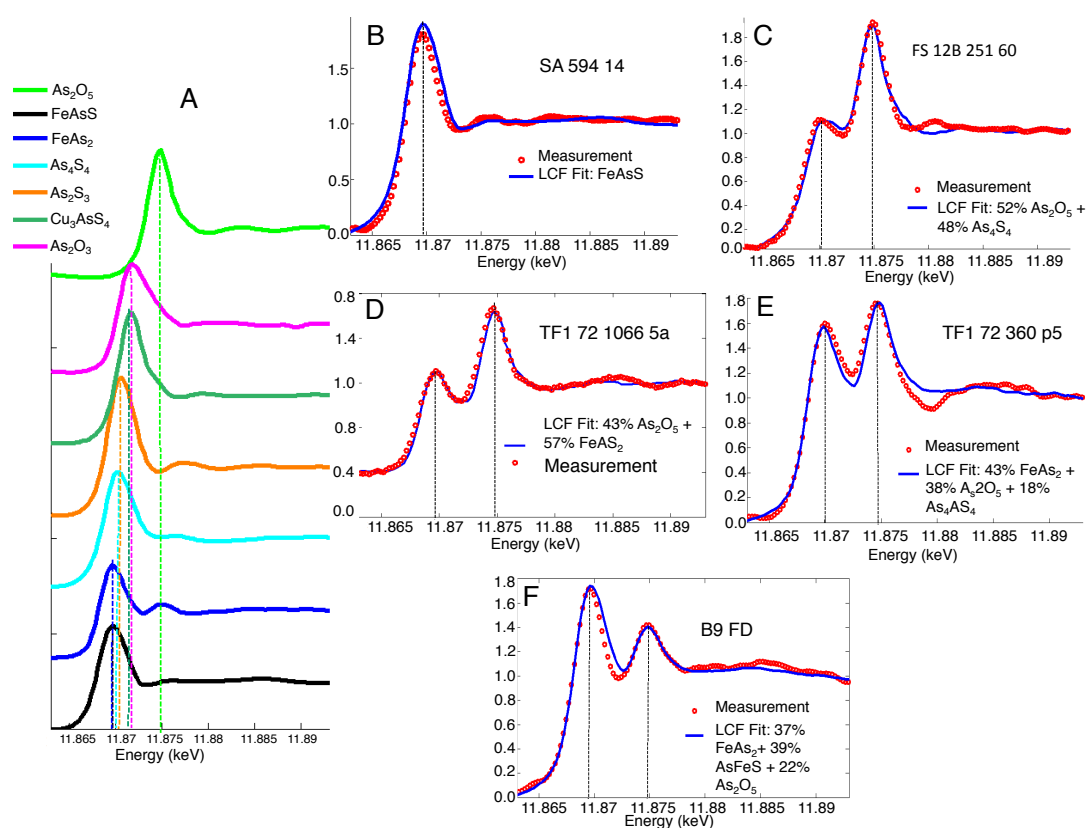


Figure S1. Examples of measured XANES spectra, including inorganic As mineral standards, samples and LCF spectra fits. A: XANES mineral standards for As sulfides, arsenate, and arsenite. These are commonly encountered in sedimentary environments arsenate = As_2O_5 and As_2O_3 = arsenite (both which bind the iron (III) oxide sink), FeAsS = arsenopyrite, FeAs_2 = Löllingite, As_4S_4 = pararealgar, As_2S_3 = orpiment, Cu_2AsS_4 = enargite (a copper sulfate mineral) (Cullen and Reimer, 1989; Smedley and Kinniburgh, 2002; O'Day, 2004). B: Example of the XANES spectrum for a 2.45 Ga sample from South Africa. C: XANES spectrum for a 1.98 Ga sample from the Zaonega formation. D-F: XANES spectra examples from 2.48 Ga (D), 2.32 Ga (E), and 2.08 Ga (F), respectively. In panels B-F the measured data are marked by red circles and the LCF fits (performed with the Athena software) are plotted in blue lines. Arsenate mineral phases were detected in 48.4% of the samples compared to only 3.2% for arsenite. Of the As-S minerals, As associated with löllingite was identified in 42% of the samples, followed by pararealgar-like phases (22.6%), arsenopyrite (12.9%), orpiment-like mineral phases (3.2%) and 0% for enargite.

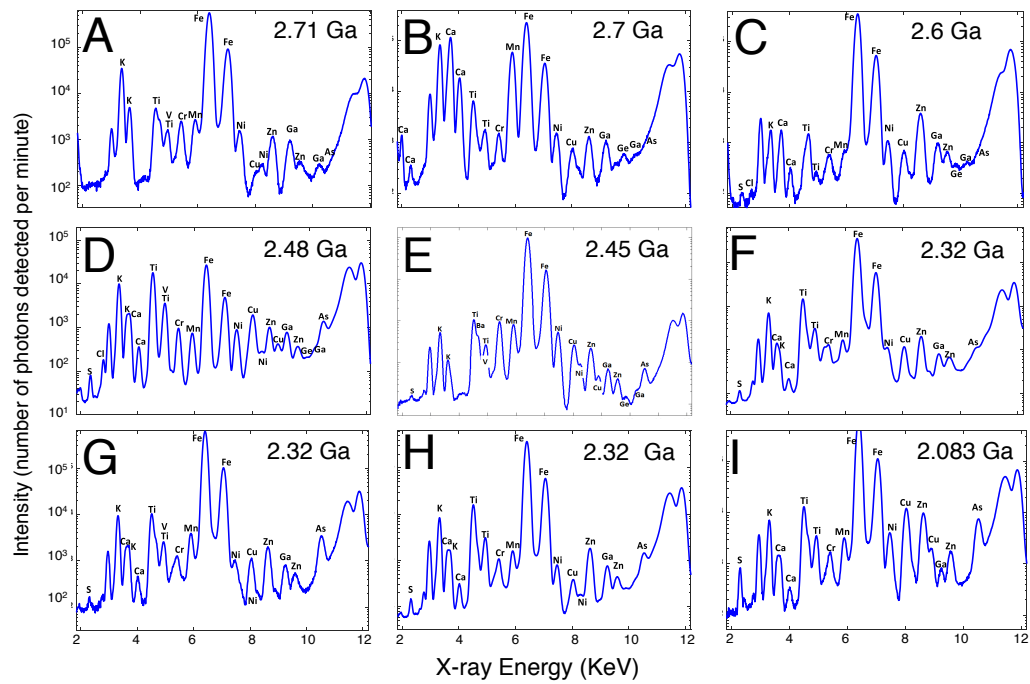


Figure S2. X-Ray Fluorescence (XRF) spectra for selected shale examples, progressing from the oldest to the youngest analyzed sediment. In the oldest samples (A-C) arsenic is below the detection limit < 1 ppm: its X-ray fluorescence peak cannot be separated from the scattered Compton background.

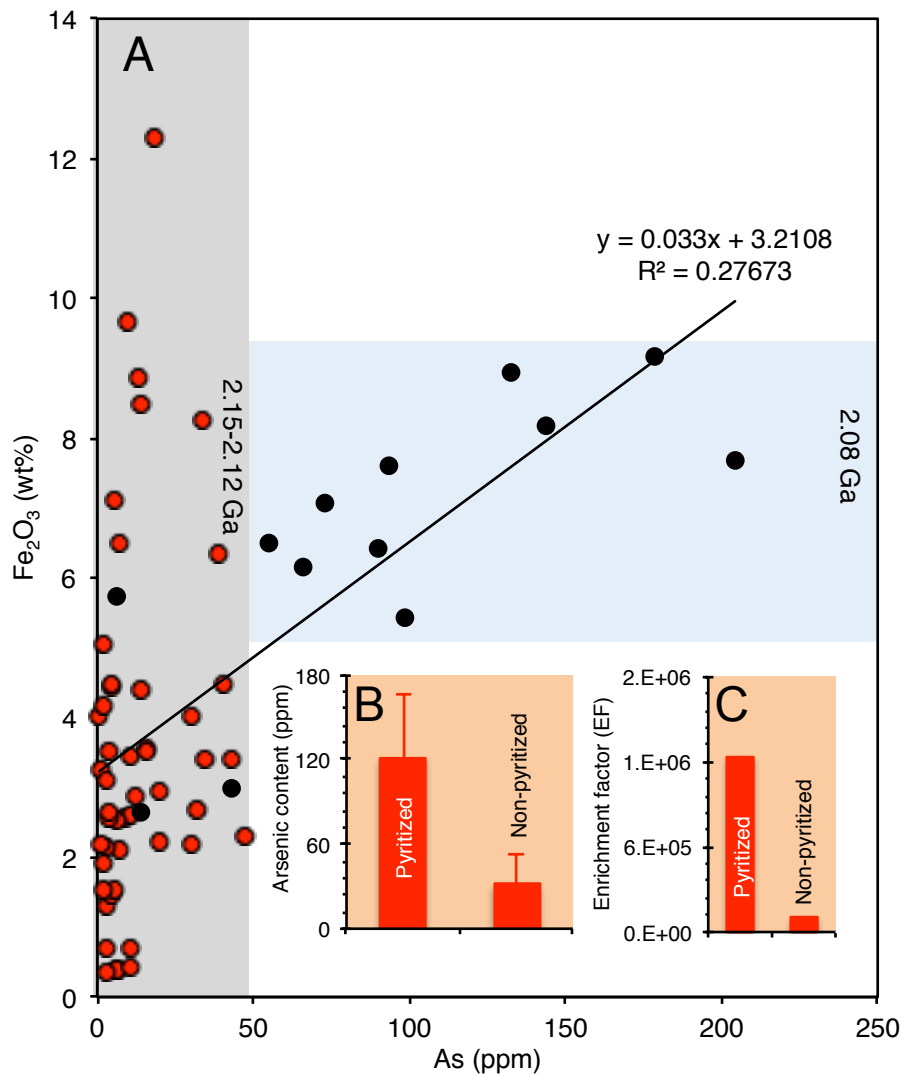


Figure S3. (A) Compiled data showing relationship between As and Fe₂O₃ (n=95) in Francevillian samples. Vertical and horizontal shading represent range of values corresponding to 2.15-2.12 Ga (red circles) and 2.08 Ga (black circles), respectively. The age model cuts up through the stratigraphy of the Francevillian Series, from the FB1a, FB1c, FB2a, FB2b, FBc and FD formations (see Canfield et al., 2013). (B) Pyritized (n=7) and non-pyritized (n=5) shales in thin pyritized shale lenses located within the predominantly non-pyritized shale deposits. (C) As enrichment factors for pyritized and non-pyritized shales relative to the upper continental crust (UCC) (McLennan, 2001), calculated as $(As/Al)_{sample}/(As/Al)_{UCC}$ (Tian and Luo, 2017). Bars in B and C are a single standard deviation from the mean. See details under supplementary discussion on arsenic cycling in Franceville. The high enrichment of As in the pyritized vs. non-pyritized shales suggests that care should be taken when individual pyrite crystals are used to infer seawater As content and provides support for data normalization to total shale Fe content.

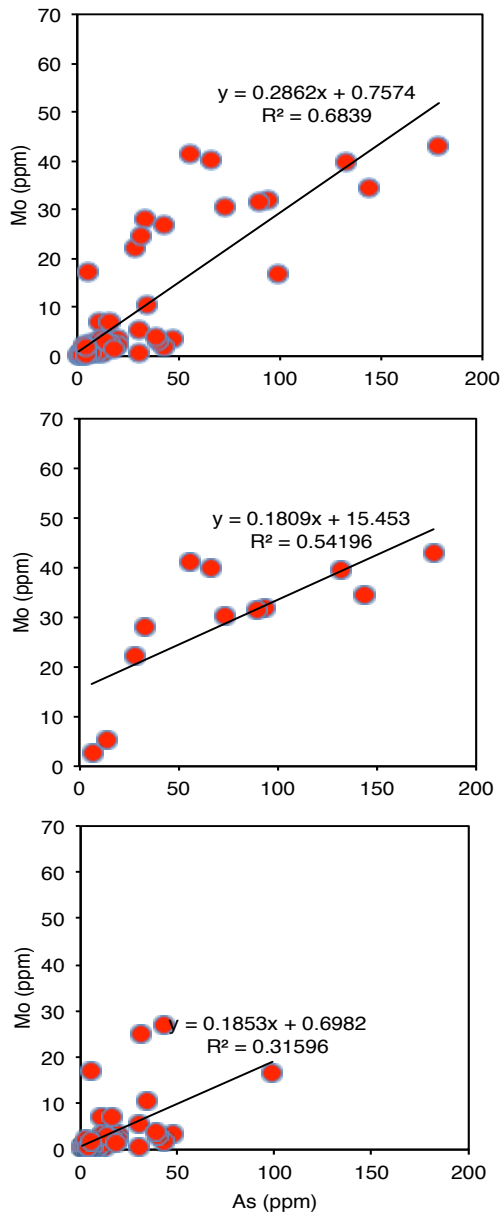


Figure S4. Relationship between Mo and As for shales in the FB, FC and FD formations of the Francevillian Series (n=95) deposited 2.15-2.08 Ga. A: Relationship between Mo and As in total dataset. B: Relationship between Mo and As deposited from sulfide-rich waters of the FD formation. C: Relationship between Mo and As deposited from the non-sulfidic waters of the FB and FC formations. See Figure 5S and Canfield et al. (2013) for a description of the stratigraphy and redox depositional reconstruction for the Franceville basin. Mo is used as a proxy for sulfidic waters (e.g., Canfield et al., 2013; Reinhard et al., 2013; Vorlicek et al., 2018). For further details, see supplementary discussion concerning arsenic cycling in the Francevillian series.

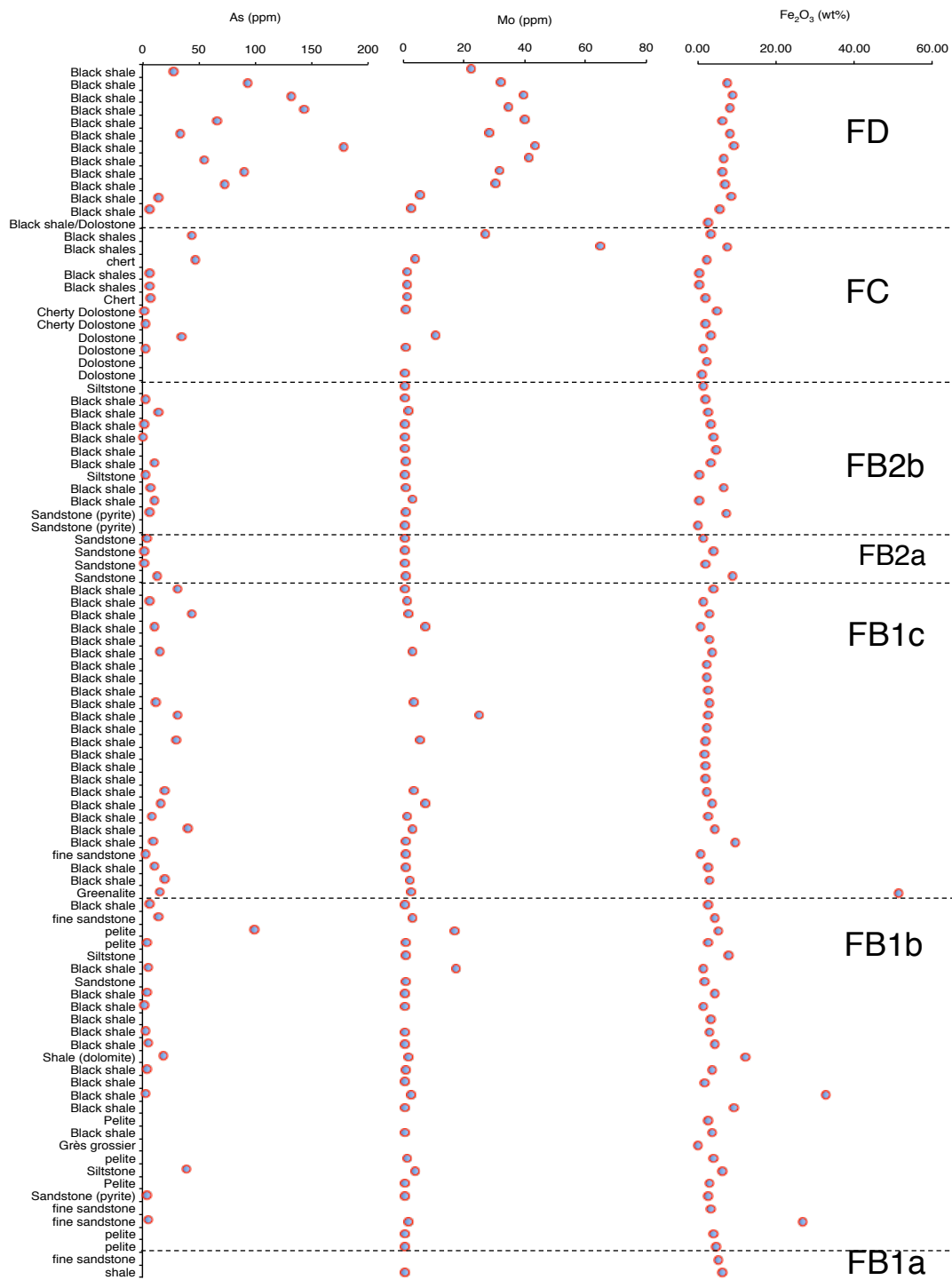


Figure S5. The stratigraphic distribution of As, Mo and Fe oxides in the Franceville Series. See Canfield et al. (2013) for a detailed stratigraphic description. Moving up section from the FB1a formation, conditions transition with changing sea levels from fully oxygenated, to mainly ferruginous/manganous in FB1c-FB1a, then to fully oxygenated in FB2a-FB2b, before transitioning to deeper sulfide-rich waters (euxinic) in the overlying, youngest FD formation (Canfield et al., 2013). Expand page size to see details.

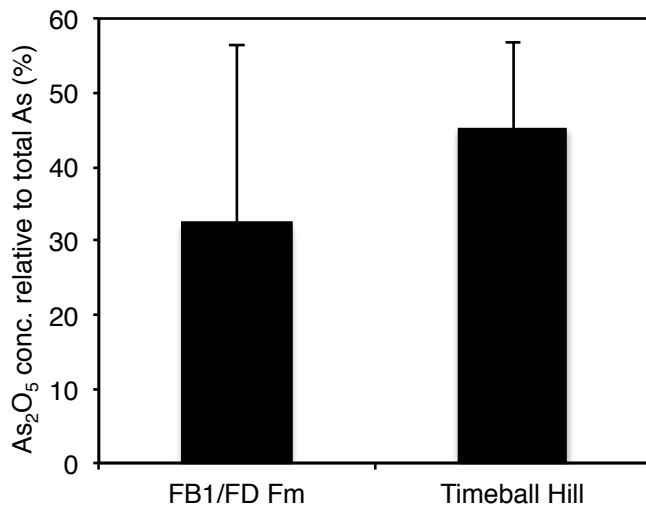


Figure S6. Average As(V) content in the FB1 and FD formation black shales compared to the GOE Timeball Hill formation black shales. Bars represent one standard deviation from the mean.

SUPPLEMENTARY INTRODUCTION

Arsenic mineralogy, sources and sinks

Of an estimated 320 As minerals known to date, only 10 are common in rocks, sediments, and soils (Henke, 2009; Foster, 2003). A bulk of these arsenic minerals exists as inorganic elemental As, arsenate, arsenic sulfides (As-S), and arsenides (e.g., NiAs_2 , $(\text{Co,Fe})\text{As}_2$, $(\text{Co,Ni})\text{As}_3$, Cu_6As , Cu_3As , $(\text{Fe,Ni,Co})\text{As}_2$, $(\text{Os,Ru})\text{As}_2$, $(\text{Fe,Ni})\text{As}$); with arsenite and arsenate minerals being the most abundant in nature (Cullen and Reimer, 1989; Maher and Butler, 1989; Smedley and Kinniburgh, 2002; Garelick et al., 2008; Henke, 2009). Typically, arsenate makes up 60% of all arsenic minerals in modern environments, As-S and sulfosalts make up 20%, followed by arsenides, elemental As, arsenite, and As in silicates and oxides, making up the remaining 20%, respectively (Garelick et al., 2008). As with most metalloids, the toxicity of As is linked to these various oxidation states.

Arsenic in rocks

Oxidative weathering, reductive dissolution of iron oxides, reactive dissolution of glass, alkaline desorption, and the dissolution of minerals containing competitive anions via desorptive anion exchange are all believed to be the primary pathways by which As is released from volcanic rocks into the hydrosphere (Smedley and Kinniburgh, 2002; Casentini et al., 2010; Banning et al., 2012; Savoie, 2013; de Sena Ferreira, 2016). In particular, the weathering of silicic volcanic rocks (e.g., felsic rocks) that are abundant in the upper continental crust, leads to arsenic mobilization (Webster et al., 2003; Price et al., 2013). For example, hydrothermal fluids associated with continental felsic magmas contain elevated levels of As (Yang and Scott, 1996; Fleet and Mumin, 1997; Muntean et al., 2011; Price et al., 2013). Most of the mineral-bound As in these volcanic rocks is associated with chalcopyrite, pyrite, arsenopyrite (FeAsS), pyrrhotite, marcasite, orpiment (As_2S_3), realgar (or pararealgar; As_4S_4), galena, sphalerite, arsenian pyrite ($\text{Fe}(\text{As,S})_2$) and various rock-forming arsenides, and to some degree silicate minerals like quartz, pyroxene and feldspars (Smedley and Kinniburgh, 2002; Garelick et al., 2008; Henke, 2009).

Oxidative dissolution of sulfide-bearing phases in these silicic volcanic rocks constitute one of the most potent pathways for the release of large quantities of As from volcanic rocks into aquatic ecosystems (see Sena Ferreira, 2016). The weathered As, in turn, either forms sedimentary As minerals through the incorporation of As into clays, carbonate minerals, or zeolites, or it is transported by rivers to the oceans where it is subsequently sequestered by various oxides, As-S minerals, or other mineral phases (Smedley and Kinniburgh, 2002; Garelick et al., 2008; Savoie, 2013; de Sena Ferreira, 2016). Accordingly – and as explained in detail below – the bulk of this As in sediments is either adsorbed onto the surface of Fe(III)(oxyhydr)oxides or substituted in sulfide and As-S minerals, depending on sulfide concentrations and the ambient seawater and pH conditions (Cullen and Reimer, 1989; Maher and Butler, 1989; Smedley and Kinniburgh, 2002; Garelick et al., 2008).

Arsenate and arsenite minerals

Arsenate (+5) and arsenite (+3) are the most common oxidation states associated with As-bearing minerals in oxygen-rich and oxygen-poor/sulfide-poor environments, respectively. The polymorphs, arsenolite and claudelite (with the chemical formula, As_2O_3) are the two most abundant arsenite minerals in nature (Henke et al., 2009). They can form following the weathering of As-S, arsenides, and elemental As minerals (Nordstrom and Archer, 2003). The moderately water-soluble arsenolite and claudelite dissolve in water to form arsenious acid (H_3AsO_3) and various ions, depending on pH.

Arsenate is a weathering product of igneous and metamorphic rocks, elemental As, As-S, and various arsenides (e.g., Westerveldite (FeAs), Sperrylite (PtAs_2), skutterudite- $(\text{Co,Ni})\text{As}_3$, Chloanthite- $(\text{Ni,Co})\text{As}_{3-x}$ (where $x=0.5-1.0$), nickline (NiAs), and löllingite (FeAs_2), amongst others (Henke, 2009)). For example, the oxidation of chloanthine produces annabergite $(\text{Ni,Co})_3(\text{AsO}_4)_2 \cdot 8\text{H}_2\text{O}$ and/or erythrine $(\text{Co}_3(\text{AsO}_4)_2 \cdot 8\text{H}_2\text{O})$ – see below for a brief discussion on how the oxidation of As-S leads to the accumulation of arsenate in the environment. Depending on pH, arsenate exists in solution as H_3AsO_4^0 , H_2AsO_4^- , HAsO_4^{2-} , or AsO_4^{3-} (Smedley and Kinniburgh, 2002; Henke, 2009). Together with the various arsenite species, these arsenate ions are the most abundant forms of As in natural waters at pH 4-10 (Cullen and Reimer, 1989; O'Day, 2006). Under these conditions, they readily bind to Fe(III)(oxyhydr)oxides to different degrees, and are subsequently removed from solution (Smedley and Kinniburgh, 2002; O'Day, 2006; Chi Fru et al., 2016a; Hemmingsson et al., 2018). It is, therefore, conceivable that during the Precambrian when banded iron formations (BIFs) were forming over large temporal and spatial scales, that the concentration of As in seawater was recorded by preferential uptake onto Fe(III)(oxyhydr)oxide surfaces. This is supported by a strong, positive linear relationship between As removal and Fe(III)(oxyhydr)oxide precipitation (Feely et al., 1991; Chi Fru et al., 2015).

Due to the chemical and physical similarity between arsenate and phosphate, arsenate can form calcium arsenate minerals ($\text{Ca}_5(\text{AsO}_4)_3(\text{OH})$) similar to apatite ($\text{Ca}_5(\text{PO}_4)_3(\text{F,Cl,OH})$). Concentrations of up to 1000 ppm As have been reported in substituted apatite minerals (Smedley and Kinniburgh, 2002; Garelick et al., 2008). These calcium arsenate minerals may be weathered from terrestrial environments in a similar manner to the oxidative weathering of apatite, which is a dominant pathway for the supply of phosphate to the oceans (e.g., Compton et al., 2000; Guidry and Mackenzie, 2000). Conversely, apatite becomes a potential As sink in sedimentary environments where it is formed, and phosphate is substituted with arsenate (Garelick et al., 2008). However, apatite is not a major mineral in our sample set, and in our study it was unlikely to have been a significant As sink.

Arsenic sulfides

Since the chemistry of As closely follows that of S, As may be substituted for S in a number of sulfide minerals (Arehart et al., 1993; Smedley and Kinniburgh, 2002; O'Day, 2004; O'Day's et al., 2006; Blanchard, 2007; Couture et al., 2013; Vaughan and Corkhill, 2017). Arsenic concentrations in sulfide minerals, such as galena, sphalerite, chalcopyrite, marcasite, pyrite, etc, can exceed 10 wt.% (Smedley and Kinniburgh, 2002; Garelick et al., 2008). The formation of these As-S minerals is promoted by conditions where $\text{pH} < 5.5$ and $\text{Eh} < 0$, and sulfide-rich conditions where As-S sulfides are stable at As concentrations $> 10^{-6.5} \text{ mol L}^{-1}$. Solid As-S phases diminish at As concentrations $< 10^{-5.3} \text{ mol L}^{-1}$ (Garelick et al., 2008). Typically, As bearing minerals in volcanic rocks and hydrothermal ore deposits form under reducing conditions and occur mostly as As-S and arsenide minerals (Henke, 2009). As discussed above, upon exposure to oxidative weathering, these minerals rapidly weather and transform into arsenite (As(III)) and arsenate (As(V)) minerals (Smedley and Kinniburgh, 2002; Henke, 2009). Similarly, sulfide minerals tend to form in reducing sedimentary environments where sufficient sulfate concentrations are present, which support sulfate-reducing microbial communities and, in turn, the generation of sulfide mineral phases. These sulfide minerals incorporate and preserve As in their crystal structures (Smedley and Kinniburgh, 2002).

Arsenopyrite, the most abundant As-S mineral in the environment, can contain As with varying oxidation states. As(V) is the major end product in oxygen-rich environments and As(III) in oxygen-poor environments. Arsenate may react with Fe(II) to form amorphous Fe(III) minerals, such as scorodite ($\text{FeAsO}_4 \cdot 2\text{H}_2\text{O}$) (Nesbitt et al., 1995; Schafuss et al., 2000; Williams, 2001; Craw et al., 2003), while some As(III) and As(V) bind to precipitating Fe(III)(oxyhydr)oxides and are rapidly removed from solution (Smedley and Kinniburgh, 2002).

Since As-S and arsenide minerals are ubiquitous in volcanic rocks comprising the upper continental crust, they would have played a key role in the supply of As to the ancient oceans during the initial rise of atmospheric oxygen (termed the Great Oxidation Event, GOE) at around 2.4 billion years ago. It has been proposed that during the GOE, a largely untapped sulfide reservoir would have been weathered as the result of increasing atmospheric oxygenation and that this would have led to the mobilization of acid soluble elements, such as Cr, in a manner akin to modern acid mine drainage (Konhauser et al., 2011). The sulfate formed was transported via rivers and groundwater to the oceans where sulfate-reducing microorganisms subsequently produced dissolved sulfide in marginal marine settings (Poulton and Canfield, 2012; Reinhard et al., 2013). Sulfide minerals precipitating from these early near-continental margin oceans, from which our samples originate, would have bound As to form various As-S minerals, such as orpiment, realgar, and arsenopyrite. These minerals were then buried in the sediment pile beneath the sulfide-rich water column. Up to 200-5000 mg/kg of As is recorded in most pyrites, with even greater amounts existing as nanoparticles in association with arsenopyrite minerals (Welch et al., 2000; Reich and Becker, 2006; Henke, 2009). In this study, we use XANES to identify and quantify the

abundance of a variety of key As-S minerals known to precipitate from sulfide-rich waters.

Arsenate and arsenite may both adsorb to Fe(III)(oxyhydr)oxides, while arsenate also commonly substitutes for phosphate and sulfate in various minerals. Typical arsenate-rich minerals (e.g., jarosite) commonly precipitate in sediments affected by acid rock drainage. This certainly may have been the case following the rise of atmospheric oxygen and the acid rock drainage suggested to have occurred immediately following the onset of the GOE (Konhauser et al., 2011). Indeed, despite never having been originally considered by the latter authors, it is likely that this process also generated a significant flux of arsenate to the oceans.

Organoarsenicals

These are not minerals per se, but instead they tend to occur in biological materials. Although organoarsenicals have been detected in waters, soils, sediments, and rocks, they are not as abundant in the geologic record as inorganic arsenates, arsenites, and As-S minerals. The sparring abundance of organoarsenicals in the geological record is probably due to the recycling of organic compounds to inorganic As phases during settling through the water column and sediment diagenesis (Cullen and Reimer, 1989; Maher and Butler, 1989; Francesconi and Kuehnelt, 2002; Smedley and Kinniburgh, 2002; Henke et al., 2009). Most notably, organic As species are only stable in very low Eh environments (Gupta and Chen, 1978; Garelick et al., 2008). Organic arsenicals are, therefore, not a primary focus of this study, but are noted as important strategies that may have enabled life to cope in early arsenic-rich oceans (Chen et al., 2017).

Redox arsenic cycling

The redox potential of the As(V)/As(III) couple, which falls between the range of $\text{NO}_3^-/\text{NO}_2^-$ and $\text{Fe}^{2+}/\text{Fe}^{3+}$, results in the oxidation of As(III) to As(V) in nature by O_2 , nitrate, and Mn oxides, through both biotic and abiotic processes (for details, see Oremland, et al., 2002a, 2002b; Toumassat et al., 2002; Budinoff et al., 2008; Kulp et al., 2008; Bhandar et al., 2012; Samantha et al., 2016; McCann et al., 2017; Zhang et al., 2017 and references therein). Particularly, the appearance of red beds in the Paleoproterozoic (Stanworth et al., 1984; Schröder et al., 2011; Bankole et al., 2016) is evidence that the $\text{Fe}^{2+}/\text{Fe}^{3+}$ redox threshold was crossed, confirming the requisite conditions for the oxidation of As(III) to As(V) were met.

The redox behavior of As in the environment is such that in anoxic sulfide-poor environments, dissolved As(III) can be oxidized by anoxygenic photosynthesizing bacteria to form As(V) (Oremland and Stolz, 2002; O'Day et al., 2004; O'Day, 2004; Budinoff et al., 2008; Kulp et al., 2008; McCann et al., 2017; Zhang et al., 2017). Under oxidizing conditions, As(III) and various arsenides that occur in volcanic rocks, are oxidized by O_2 and MnO_2 to As(V) (see for example, Oremland, et al., 2002a, 2002b; Toumassat et al., 2002; Samantha et al., 2016 and references therein). In sulfide-rich environments,

As-S minerals form, removing As from solution (O'Day et al., 2004; O'Day, 2004; Godelitsas et al., 2015). In the presence of oxygen, As(V) forms through the oxidation of As-S minerals (e.g., Corkhill and Vaughan, 2009). While abiotic photochemical oxidation of As(III) has been reported (e.g., Brockbank et al., 1998; Bhandar et al., 2012), this was likely not a prominent driver of As oxidation in the Precambrian oceans (discussed in more details below). Finally, arsenate (V) reduction is mostly a biological process that requires organic carbon as an electron donor for the reduction of As(V) to As(III) under anoxic settings (Oremland and Stolz, 2002; Silver and Phung, 2005).

SUPPLEMENTARY DISCUSSION

Seawater arsenic to iron content and arsenic speciation

We used reference As minerals for XANES analysis to identify various As species associated with well-known As phases formed under different redox conditions in the samples. The data indicate that As is present in the samples mainly as As(V) and as various As-S minerals phases, but rarely (in one sample) as As(III) and As-S; enargite was not detected (Fig. S1 and Table S1). The iron formation (IF) record constrains the relationship between As and the Fe in oxyhydroxide sinks (As/Fe ratios), as well as oxidative weathering (As/Ti ratios) across the sampled interval, indicating a homogenous behavior between Fe and As in both records. By contrast, the shale sample set provides comprehensive information on the As(V) and As sulfide distribution in the sample set, which would not have been the case for the sulfide-poor IF record.

Both the shale and IF records display a marked drop towards lower values at the Archean Proterozoic boundary, followed by a constriction towards the maximum, in the Paleoproterozoic, coinciding with the rise of atmospheric oxygen. This suggests that the As content in the water column and sediments, with respect to Fe, were behaving in a similar and co-dependent manner before and after the Archean-Paleoproterozoic transition. Moreover, the data further show that until 2.0 Ga, the As/Fe molar ratio was mostly constant, with a bulk of the data remaining in the range recorded during the Neoproterozoic (Fig. 1A). This suggests that dilution or excessive enrichment of sedimentary As, resulting from rapid fluctuations in sedimentary Fe content, was negligible across the Archean-Proterozoic boundary. The consistency of the As(V) and As-S content recorded at 2.0 Ga with the GOE levels, despite a spike in the As/Fe molar ratio at this time relative to the immediate GOE, further suggests that rapid changes in the Fe reservoir did not compromise As speciations, the sedimentary archive, and content of the recorded seawater As species.

Hydrothermal fluids would have contributed significant amounts of arsenic to the ocean during the Precambrian when hydrothermal activity could have been up to 3 times higher than at present (e.g., Martin et al., 2008). But according to Figure 1B, sedimentary arsenic content increases dramatically following the GOE transition by several orders of magnitude. Given that it is thought that hydrothermal activity was declining from the Archean through the Proterozoic eon (See for example Chi Fru et al., 2016b), a predominantly hydrothermal source for the observed rise in marine arsenic content across the Archean-Proterozoic boundary cannot explain the sudden rise in sedimentary arsenic content we see following the GOE transition, if it is true that hydrothermal activity decreased from the Archean through the Proterozoic eon to the much lower Phanerozoic activity. Moreover, the arsenic speciation data are from near continental margin setting deposits, some of which have been argued to have experienced limited hydrothermal influence (Canfield et al., 2013; Ngombi-Pemba et al., 2014), with a

main source for sediments supply being the continents. We show in our Figure 2A that oxidative weathering of the continents became a more important source of arsenic to marine waters following the rise of atmospheric oxygen. Today, more than 80% arsenic supply to seawater originates from continental weathering, rather than hydrothermal activity. Hence what the data show is that despite this transition from mainly hydrothermal supply of As to the ocean to increasing continental sourcing, the iron reservoir was not affected enough to skew the sequestration of As by iron; Fe(III)(oxyhydr)oxides in the case of BIFs and Fe sulfides in the shale record.

As/Fe and As/Ti ratios in the GOE and NOE IFs

During the Neoproterozoic Sturtian glaciations, IFs were formed by the submarine hydrothermal sourcing of iron under restricted conditions (Hoffman et al., 1998). The oceans would have been effectively isolated from a terrestrial sediment supply and the atmosphere, thereby enabling the ocean stratification and anoxic conditions required for the deposition of the Neoproterozoic IFs (Hoffman et al., 1998). Importantly, the IFs associated with the Sturtian Snowball Earth were deposited before the terminal rise in atmospheric oxygen to near modern-day levels during the late Neoproterozoic. At this time, oxidative weathering may have been muted relative to conditions during the deposition of Paleoproterozoic IFs that were deposited in the lead up, and coincident with the GOE, when oxygen may have approached present atmospheric levels (see Lyons et al., 2014 for a review). After the GOE, atmospheric oxygen levels declined to relatively low levels during the mid-Proterozoic. This explains the muted NOE As/Ti ratios recorded for the Neoproterozoic Sturtian IFs and possibly their accompanying As/Fe ratios.

According to Chi Fru et al. (2015), although oxidative weathering enabled the increased supply of As to the oceans from land across the GOE boundary, the effectiveness of this oxidative supply of As was hampered by continental ice coverage. Therefore, the rise in As/Ti ratios in IFs deposited at the onset of the GOE can be considered as indicative of the onset of As-induced oxidative weathering, while the muted As/Fe ratios indicate that the amount of As reaching the ocean did not increase substantially relative to the Fe reservoir.

Arsenic cycling in Franceville

In Francevillian samples, As was below the detection limit in several samples with elevated Fe₂O₃ but present at, or above, detectable levels in numerous samples with extremely low Fe₂O₃ content. This weak correlation between As and Fe₂O₃ content (Fig. S3A) was observed regardless of whether the shale sample was pyrite-rich (2.08 Ga) or pyrite-poor (2.15-2.12 Ga). Importantly, the poor correlation between Fe₂O₃ and bulk As content cannot be ascribed to diagenesis, because the post-depositional reduction of Fe(III) would have resulted in a linear loss of both Fe and As to sediment pore waters.

The lag in the rise of As observed in shales at 2.15-2.12 Ga, when the Fe₂O₃ sink parallels that of the 2.08 Ga As-rich shales (Fig. S3A), hints that either the supply of dissolved As(V) from land was naturally low at 2.15-2.12 Ga or that some intrinsic property, e.g., seawater sulfide levels (Fig. S4-S5), controlled quantitative As(V) precipitation out of seawater. For example, Figure S4A-C shows a positive relationship between Mo—a sulfidic water column proxy—and As

for 95 samples aged 2.15-2.08 Ga, where an up to 68% ($R^2=0.6839$) total covariation is seen between As and Mo (Fig. S4A) in the total sample set, 54% ($R^2=0.5496$) for shales formed from sulfidic waters (Fig. S4B) and a weak ~32% ($R^2=0.31596$) covariation for shales formed from non-sulfidic samples (Fig. S4C). As expected, the sulfide-rich waters of the FD formation that were overlain by oxic waters show the strongest relationship between Mo and As, indicating that as in modern environments, sulfide played a strong influence on the removal of As from seawater (e.g., Cullen and Reimer, 1989; Smedley and Kinniburgh, 2002; O'Day et al., 2004; O'Day, 2006; Godelitsas et al., 2015). Nonetheless, a stratigraphic reconstruction shows limited variability in Fe_2O_3 distribution up the Franceville Series, between 2.15 to 2.08 Ga. These distributions, together with the more positive correlation between Fe_2O_3 and As in the redox stratified FD formation of the Franceville Series at 2.08 Ga (Fig. S3A), indicate a likely change in As supply dynamics from the continent to the oceans. Our observed increase in water column sulfide content and the muted rapid fluctuations in the iron oxide sink, suggests that continental-weathering dynamics and redox change, promoted the enrichment of As in the sediments at 2.08 Ga. If this were not the case, a dynamic spike in As would be expected when conditions became ferruginous and manganous in the underlying FB1a-FB1c formation (Canfield et al., 2013; Fig. S5).

It is also possible that As(V) was microbially reduced with organic matter to As(III), but we have no evidence that can support this possibility. However, elevated organic matter and As(V) accumulation at 2.08 Ga comes after a period of rapid sedimentation and reduced organic matter burial at 2.1 Ga (Canfield et al., 2013; Reynaud et al. 2017).

Biological retention of As in the fully oxygenated FB2 formation seawater would have considerably decreased total sediment As, As(III), and As(V) content, as reflected by individual low sediment contents at this time. Importantly, hydrothermal activity apparently had a negligible influence on seawater properties in the Paleoproterozoic Francevillian Ocean (Ngombi-Pemba et al., 2014), indicating that the bulk of dissolved As would have been supplied to the oceans via riverine input; a process which supplies up to 82.4% of As to the modern ocean (Henke, 2009). This would have brought As(V) from the hinterlands into direct contact with the epicontinental marine phytoplankton community that ventilated the Francevillian sea margin, a paleo-environment proposed to have hosted the first purported O_2 -respiring colonial organisms (El Albani et al., 2010, 2014).

Locally, the ~2.1 Ga oxic FB1 and 2.08 Ga sulfidic FD deposits (Fig. S5), record average As(V) levels that are 1.4 times less than the sulfidic GOE Timeball Hill black shales that formed at 2.32 Ga in a stratified marginal ocean similar to the FD formation (Fig. S6). This may imply smaller quantities of As(V) were reaching the 2.2-2.08 Ga sediments relative to those formed at 2.32 Ga. Similarly, average sedimentary As(V) archives from the 2.2-2.08 Ga Francevillian samples are comparable to the 2.32 Ga average, hinting that surface ocean As cycling by phytoplankton activity may have been stable, but more intense at 2.32 Ga—as indicated by a smaller standard deviation from the mean values (Fig. S6)—compared to ~120-237 million years later in the Francevillian basin.

Post-depositional As cycling across the Archean-Proterozoic boundary

Regardless of whether As-S enrichment during and after the GOE was diagenetic or of seawater origin, either scenario can occur only if sulfate concentrations and bacterial sulfide production were elevated, relative to the preceding time period. Intuitively, seawater sulfate concentrations are expected to have fluctuated proportionately with atmospheric O₂ content (Poulton and Canfield, 2011; Planavsky et al., 2012; Scott et al., 2014), and as such, As concentrations in chemical sediments should scale with the rise in O₂ and corresponding increase in seawater sulfate. Lower levels of As(V) in Archean shales, when the environment was more reducing than the Paleoproterozoic and hence more favorable for anaerobic bacterial As(III) oxidation, argues against diagenetic anaerobic oxidation being the major source of elevated As(V) during the GOE. This would hold true unless anaerobic bacterial As(III) oxidation evolved during the GOE, an assertion that runs contradictory to previous predictions (Oremland and Stolz, 2003; Sforza et al., 2014). Similarly, no known post-depositional transformation (diagenetic or metamorphic) is known that can explain the enrichment of As(V) in the sediments, other than the rise and enrichment of As(III) oxidants in the anoxic sediments that would have allowed biological transformation of As(III) to As(V) (Oremland and Stolz, 2002). In all scenarios, post-depositional formation of As(V) would only occur if, for example, marine nitrate content, whose concentration is tightly controlled by oxygen availability (Zerkle et al., 2017), increased to enable for example anaerobic microbial transformation of As(III) to As(V) in the sediments. In summary, all the data point to both the enrichment of As-S and As(V) across the GOE to the rise of atmospheric oxygen. Finally, modern evidence suggest that following the removal of arsenic from seawater, at most 25% can be lost due to diagenetic burial processes. However, this loss is not expected to compromise the original temporal and spatial trend (e.g., Feely et al. 1991; Chi Fru et al. 2015).

Photochemical As oxidation across the Archean-Proterozoic boundary

The photochemical oxidation of As(III) to As(V) by UV light requires molecular O₂ (Emett and Khoe, 2001; Hug et al., 2001, 2003; Dutta et al., 2005; Neppolian et al., 2008; Bhandari et al., 2012), although some degree of anoxic photo-oxidation has been experimentally observed (Brockbank et al., 1998). Accordingly, the magnitude of a potential photochemical contribution to seawater As inventories remains unclear. However, conceptually the photochemical oxidation of As(III) is unlikely to be a significant source of sediment bound As(V), otherwise a strong spike should be recorded during the Archean when the ocean surface was subjected to unattenuated fluxes of UV irradiation (Walker, 1977; Kasting and Donahue, 1980).

Implications for biological arsenic cycling and phosphate uptake

Chemolithoautotrophs and the Oxyphotobacteria living in arsenate-replete ecosystems switch on a high affinity phosphate uptake transport system (Pst) when dissolved arsenate to phosphate ratios exceed a certain level, in order to discriminate arsenate from phosphate (e.g., Thiel, 1988; Dyhrman and Haley, 2011; Elias et al., 2012). This is the result of the physicochemical similarity between arsenate and phosphate imposing an artificial phosphate limitation, leading to photosynthetic activity being inversely related to seawater arsenate content (see reviews by Cullen Reimer, 1989; Smedley and Kinniburgh, 2002).

It has been proposed that the earliest life forms emerged around hydrothermal/geothermal ecosystems and that the Precambrian oceans were generally up to three times more hydrothermally active than the modern oceans (Martin et al., 2008; Mulkidjanian et al., 2012). Hydrothermal fluids, both marine and terrestrial, contain some of the highest natural concentrations of arsenic recorded in any aqueous systems on Earth (Price et al., 2013; Breuer and Pichler, 2013). Importantly, the distribution of arsenic detoxification across the entire tree of life, including some of the most primitive lineages, suggests that exposure to arsenic is primordial (Gihring et al., 2003; Jackson and Dugas, 2003; Qin et al., 2006; Ye et al., 2012; Chi Fru et al., 2015; Chen et al., 2017; Tian and Luo, 2017; Hoffman et al., 2018). Life, therefore, likely had to develop mechanisms to deal with arsenic very early on in its history (Jackson and Dugas, 2003; Chen et al., 2017). Indeed, the continuous expression of arsenic detoxification in modern organisms, and in recently evolved lineages, indicate that arsenic is still a threat for the organization of life in the biosphere.

It appears that arsenic detoxification systems were imperative for the evolution and establishment of life as we know it in the biosphere. This is because protection or detoxification mechanisms against arsenic toxicity are widespread across all the three domains of life, from simple prokaryotes to advanced eukaryotes (e.g., Meharg, A.A., and Hartley-Whitaker, J., 2002; Ghosh et al., 1999; Chen et al., 2016; Hao et al., 2017). These organisms employ an assortment of energy-expensive detoxification mechanisms that cells would get rid of if they were not important for their ecological success and dominance. Some of these pathways have evolved by convergent evolution to carry out the same function (e.g., Qin et al., 2007) and have been transferred horizontally across distantly related lineages (e.g., Chen et al., 2017), suggesting that the maintenance against the detrimental effects of arsenic across all the three domains of life is an ecological challenge that life had to surmount in order to establish ecological dominance.

A valid question to ask then is what promoted the innovation of the various arsenic protection strategies and whether their invention played a major role in shaping the survival of life in the natural environment? Answers to this persisting puzzle requires a chronology of marine arsenic dynamics and speciation through Earth history in order to calibrate when such processes would have emerged in the ocean and when they would have been critical for the survival of extant life. For instance, there is new evidence that sedimentary arsenic content was much higher at the terminal end of Earth's Snowball glaciations, coinciding with the emergence and radiation of the Ediacaran biota and that Precambrian and Early Phanerozoic marine arsenic content was generally higher than in the present ocean (Chi Fru et al., 2015; Tian et al., 2017). Our Figure 2 certainly supports the latter. Taken together, life would have had to handle this high arsenic loading through a natural selection process, the expression of which is what we observe

as arsenic cycling gene expression in the modern marine biosphere. For example, bacterial communities have evolved remarkable arsenic detoxification pathways that they, in turn, use to kill and gain advantage over other microorganisms, as well as prevent being eaten by protists (Hao et al., 2017; Chen et al., 2018).

It was recently demonstrated that the distribution of sulfide minerals and Fe(III)(oxyhydr)oxides in a hydrothermal setting controls the distribution of dissolved As, phosphate, As resistance genes, and As respiration and oxidizing genes (Chi Fru et al., 2018). Importantly, modern hydrothermal environments are believed to represent examples of the hostile environments in which Precambrian microbial life evolved and thrived, as mentioned above. In line with this idea, Chi Fru et al. (2018) found that sulfide depositing hydrothermal settings are enriched in phosphate. This appears to reduce microbial phosphate stress as indicated by a microbial population containing a genomic composition that is low in high affinity phosphate uptake. High affinity phosphate uptake genes are required by cells when environmental phosphate concentrations are low or when arsenate to phosphate ratios are high (Elias et al., 2012). In contrast, an elevated density of high affinity phosphate uptake gene abundance in Fe(III)(oxyhydr)oxides-depositing settings suggests these types of environments are phosphate stressed (Chi Fru et al., 2018). Similarly, populations in the sulfide-rich settings exhibit a lower abundance of arsenic resistance and metabolic genes, relative to the Fe(III)(oxyhydr)oxide-rich settings. This discrepancy in genetic abundance of As cycling genes in the sulfide-rich habitats is related to rapid As removal by precipitating sulfide and As-S minerals with low solubility product constants.

Collectively, these data suggest that the emergence of large-scale deposition of As-S in the early oceans following the GOE, together with widespread deposition of Fe(III)(oxyhydr)oxides in association with IFs, would have dramatically affected the spatial assemblage of microbial communities as a function of their ability to resist As toxicity. Moreover, increasing aqueous arsenate/phosphate ratios may have caused phosphate biolimitation because of the chemical similarity existing between arsenate and phosphate. As a consequence, arsenate is taken up in the place of phosphate into the cell when arsenate to phosphate ratios are high (Rothstein, 1963; Elias et al., 2012). In the photic zone of modern oceans, increasing arsenate to phosphate ratios diminish primary productivity (e.g., Cullen and Reimer, 1989; Smedley and Kinniburgh, 2002; Dyhrman and Haley, 2011). Therefore, the global emergence of As-S and arsenate in the oceans following the rise of atmospheric oxygen would have had strong consequences for life, the true impact and ramifications which remain to be quantified. However, the current work sets a firm foundation on which such research would be based.

SUPPLEMENTARY METHODS

XANES analysis

The samples analysed in this study were chosen based on previous studies where they have been used for constructing Precambrian seawater and atmospheric composition because of limited post-depositional modification (Bekker et al., 2010; Kendall et al., 2010; Canfield et al., 2013; Ngombi-Pemba et al., 2014; Chi Fru et al., 2015, 2016b). The XANES measurements were performed on homogenized powdered samples at the Nanoscopium beamline Synchrotron Soleil facility, France (Somogyi et al., 2015), using a Si(111) double crystal monochromator with an unfocused $2 \times 2 \text{ mm}^2$ X-ray beam. The As K-edge was scanned in the 11.862-11.8970 keV energy range, at 0.25 eV steps. Natural

minerals of known As oxidation states, arsenopyrite (FeAsS), löllingite (FeAs₂), realgar (As₄S₄), orpiment (As₂S₃), enargite (Cu₃AsS₄), fetiasite (Fe²⁺, Fe³⁺, Ti⁴⁺)₃O₂ As³⁺₂O₅), and legrandite (Zn₁₄(OH)(AsO₄)₉·12H₂O), were measured as As-XANES model compounds. These minerals provide a good representation of As speciation and oxidation states predominant in nature. The XANES standards were measured regularly, at least once after 12 hours. The FeAsS, FeAs₂, As₄S₄, As₂S₃, and As₂O₅ standards, chosen by principal component analysis (PCA) of the XANES data-set of the samples and target transformation of the standards were used for XANES data fitting with the Athena Software package. XANES measurements, in fluorescence yield mode registered full XRF spectra at each energy step by a KETEK Si drift diode detector (SDD) having a 50 mm² active surface and allowed the detection of trace amounts of As. The PyMCA software (Solé et al., 2007) was used to subtract background from the XRF signal, resulting in XANES spectra recovered at ppm level As concentrations. The stability of the individual XANES spectra over ~5 min measurement time confirmed the absence of photo-oxidation and photo-reduction of As during measurements. The averaged XANES improved the spectral quality with better signal/noise ratio and was used for XANES data fitting with the ATHENA software. Quantitative information on the relative proportions of the modeled As oxidation states were obtained by linear combination fit (LCF) of the XANES sample spectra with known standards. Due to the similarity of the individual XANES spectra of the different As-S (FeAsS, FeAs₂, As₄S₄, and As₂S₃), the accuracy of the estimated relative individual sulfide proportions in the samples is estimated to be c. 20-30%. However, due to the significant energy separation of their absorption edges and white lines, the total As-S pool can be unambiguously distinguished from As(III) and As(V) oxides and their relative proportions can be quantified with ~15 % error (usually associated to LCF procedure, Foster and Kimm, 2014), which was our goal. Whole-rock geochemical analyses of major and trace elements were performed on selected samples.

IF analysis and literature data collection

1. Bulk BIF solution analysis was performed at the European Institute for Marine Studies, Laboratoire Domaines Océaniques, Technopôle Brest-Iroise, France. For total digests, ~50 mg was sequentially digested in a concentrated HF-HNO₃ mixture, followed by aqua regia, and finally 6M HCl. Samples were then taken up with 2% HNO₃ and analyzed for trace element concentrations on a Thermo Scientific Element2 High Resolution Inductively Coupled Plasma Mass Spectrometer. Indium was monitored as an internal standard. Multi-element solutions were used to calibrate the mass spectrometer and several geostandards (BHVO-2, IF-G, and GL-O) were put through the entire digestion treatment to monitor external reproducibility. Bulk digestion and laser ablation analyses performed at the University of Alberta was as previously described (Konhauser et al., 2009, 2011; Robbins et al., 2013). Literature survey data were obtained from references listed as 2-27, below.
2. Konhauser, K.O., Pecoits, E., Lalonde, S.V., Papineau, D., Nisbet, E.G., Barley, M.E., Arndt, N.T., Zahnle, K., and Kamber, B.S., 2009, Oceanic nickel depletion and a methanogen famine before the Great Oxidation Event: *Astrobiology*, v. 458(7239), p. 750–753.
3. Konhauser, K.O., Lalonde, S.V., Planavsky, N.J., Pecoits, E., Lyons, T.W., Mojzsis, S.J., Rouxel, O.J., Barley, M.E., Rosière, C.A., Fralick, P.W.,

- Kump, L.R., and Bekker, A., 2011, Aerobic bacterial pyrite oxidation and acid rock drainage during the Great Oxidation Event: *Astrobiology*, v. 478(7369), p. 369–373.
4. Noah Planavsky (Yale University), personal communication of previously unpublished data.
 5. Mloszewska, A.M., Pecoits, E., Cates, N.L., Mojzsis, S.J., O'Neil, J., Robbins, L.J., and Konhauser, K.O. 2012, The composition of Earth's oldest iron formations: The Nuvvuagittuq Supracrustal Belt (Québec, Canada): *Earth and Planetary Science Letters*, v. 317-318, p. 331-342, doi: 10.1016/j.epsl.2011.11.020.
 6. Dymek, R., and Klein, C. 1988, Chemistry, petrology and origin of banded iron-formation lithologies from the 3800 Ma Isua supracrustal belt, West Greenland: *Precambrian Research*, v. 39(4), p. 247–302, doi: 10.1016/0301-9268(88)90022-8.
 7. Bhattacharya, H.N., Chakraborty, I., Ghosh, K.K. 2007, Geochemistry of some banded iron-formations of the Archean supracrustals, Jharkhand-Orissa region, India: *Journal of Earth System Science*, v. 116(3), p. 245-259.
 8. Lascelles, D.F. 2006, The Mount Gibson banded iron formation-hosted magnetite deposit: two distinct processes for the origin of high-grade iron ore. *Economic Geology*, v. 101(3), p. 651-666, doi: 10.2113/gsecongeo.101.3.651.
 9. Klein, C., and Ladeira, E.A. 2000, Geochemistry and petrology of some Proterozoic banded iron-formations of the Quadrilátero Ferrífero, Minas Gerais, Brazil: *Economic Geology*, v. 95(2), p. 405-428, doi: 10.2113/gsecongeo.95.2.405.
 10. Gross, G.A. 2009, Iron Formation in Canada, Genesis and Geochemistry. Geological Survey of Canada, Open File 5987.
 11. Alibert, C., and McCulloch, M.T. 1993, Rare earth element and neodymium isotopic compositions of the banded iron formations and associated shales from Hamersley, western Australia: *Geochimica et Cosmochimica Acta*, v. 57(1), p. 187-204, doi: 10.1016/0016-7037(93)90478-F.
 12. Beukes, N.J., and Klein, C. 1990, Geochemistry and sedimentology of a facies transition from microbanded to granular iron-formation in the early Proterozoic Transvaal Supergroup, South Africa: *Precambrian Research*, v. 47(1-2), p. 99-139, doi: 10.1016/0301-9268(90)90033-M.
 13. Klein, C., and Beukes, N.J. 1989, Geochemistry and sedimentology of a facies transition from limestone to iron-formation deposition in the Early Proterozoic Transvaal Supergroup, South Africa: *Economic Geology*, v. 84(7), p. 1733-1774, doi:10.2113/gsecongeo.84.7.1733.
 14. Spier, C.A., de Oliveira, S.M.B., Sial, A.N., and Rios, F.J. 2007, Geochemistry and genesis of the banded iron formations of the Cauê Formation, Quadrilátero Ferrífero, Minas Gerais, Brazil: *Precambrian Research*, v. 152(3-4), p. 170-206, doi: 10.1016/j.precamres.2006.10.003.
 15. Slack, J.F., Grenne, T., and Bekker, A. 2009, Seafloor-hydrothermal Si-Fe-Mn exhalites in the Pecos greenstone belt, New Mexico, and the redox state of ca. 1720 Ma deep seawater: *Geosphere*, v. 5(3), p. 302-314, doi: 10.1130/GES00220.1.
 16. Hatton, O.J., and Davidson, G.J. 2004, Soldiers Cap Group iron-formations, MT Isa Inlier, Australia, as windows into the hydrothermal evolution of a base-metal-bearing Proterozoic rift basin: *Australian Journal of Earth Sciences*, 51(1), 85-106, doi:10.1046/j.1400-0952.2003.01047.x.
 17. McClung 2006 PhD thesis

18. Klein, C., and Beukes, N.J. 1993, Sedimentology and geochemistry of the glaciogenic late Proterozoic Rapitan iron-formation in Canada: *Economic Geology*, v. 88(3), p. 542-565, doi: 10.2113/gsecongeo.88.3.542.
19. Klein, C., and Ladeira, E.A. 2004, Geochemistry and mineralogy of Neoproterozoic banded iron-formations and some selected, siliceous manganese formations from the Urucum district, Mato Grosso do Sul, Brazil: *Economic Geology*, v. 99(6), p. 1233-1244, doi: 10.2113/gsecongeo.99.6.1233.
20. Lottermoser, B.G., and Ashley, P.M. 2000, Geochemistry, petrology and origin of Neoproterozoic ironstones in the eastern part of the Adelaide Geosyncline, South Australia: *Precambrian Research*, v. 101(1), p. 49-67U, doi: 10.1016/S0301-9268(99)00098-4.
21. Davidson, G.J., Stolz, A.J., and Eggins, S.M. 2001, Geochemical anatomy of silica iron exhalites: evidence for hydrothermal oxyanions cycling in response to vent fluid redox and thermal evolution (Mt. Windsor Subprovince, Australia): *Economic Geology*, v. 96(5), p. 1201-1226, doi: 10.2113/gsecongeo.96.5.1201.

22. Duhig, N.C., Stolz, J., Davidson, G.J. and Large, R.R. 1992, Cambrian microbial and silica gel textures in silica iron exhalites from the Mount Windsor Volcanic Belt, Australia: Their petrography, chemistry, and origin: *Economic Geology*, v. 87(3), p. 764-784, doi: 10.2113/gsecongeo.87.3.764.
23. Grenne, T., and Slack, J.F. 2005, Geochemistry of jasper beds from the Ordovician Løkken Ophiolite, Norway: Origin of proximal and distal siliceous exhalites: *Economic Geology*, v. 100(8), p. 1511-1527, doi:10.2113/100.8.1511.
24. Guerrak, S. 1988, Geology of the Early Devonian oolitic iron ore of the Gara Djebilet field, Saharan Platform, Algeria: *Ore Geology Reviews*, v. 3(4), p. 333–358, doi:10.1016/0169-1368(88)90026-1.
25. Leistel, J.M., Marcoux, E., and Deschamps, Y. 1998, Chert in the Iberian Pyrite Belt: *Mineralium Deposita*, v. 33(1-2), p. 59-81.
26. Hein, J.R., Yeh, H.-W., Gunn, S.H., Gibbs, A.E., and Wang, C.-H. 1994 Composition and origin of hydrothermal ironstones from central Pacific seamounts: *Geochimica et Cosmochimica Acta*, 58(1), 179-189, doi: 10.1016/0016-7037(94)90455-3.
27. Hrischeva, E., and Scott, S.D. 2007, Geochemistry and morphology of metalliferous sediments and oxyhydroxides from the Endeavour segment, Juan de Fuca Ridge: *Geochimica et Cosmochimica Acta*, v. 71(14), p. 3476-3497, doi: 10.1016/j.gca.2007.03.024.

REFERENCES

- Arehart, G.B., Chryssoulis, S.L., and Kesler, S. 1993, Gold and arsenic in iron sulfides from sedimented-hosted disseminated gold deposits: implications for depositional processes: *Economic Geology*, v. 85, p. 171–185, doi:10.2113/gsecongeo.88.1.171.
- Bankole, O.M., El Albani, A., Meunier, A., Rouxel, O.J., Gauthier-Lafaye, F., and Bekker, A. 2016, Origin of red beds in the Paleoproterozoic Franceville Basin, Gabon, and implications for sandstone-hosted uranium mineralization: *Journal of American Science*, v. 316(9), p. 839–872, doi: 10.2475/09.2016.02.
- Banning, A., Cardona, A., and Råde, T.R. 2012, Uranium and arsenic dynamics in volcano-sedimentary basins – An exemplary study in North-Central Mexico: *Applied Geochemistry*, v. 27(11), p. 2160–2172, doi:10.1016/j.apgeochem.2012.01.001.
- Bekker, A., Holland, H.D., Wang, P.-L., Rumble III, D., Hannah, J.L., Coetsee, L.L., and Beukes, N.J. 2004, Dating the rise of atmospheric oxygen: *Nature*, v. 427, p. 117–120.
- Bhandari, N., Reeder, R.J., and Strongin, D.R. 2012, Photoinduced oxidation of arsenite to arsenate in the presence of goethite: *Environmental Science and Technology*, v. 46. P. 8044–8051, doi:10.1021/es300988p.
- Blanchard, M., Alfredsson, M., Brodholt, J., Wright, K., Catlow, R.A. 2007, Arsenic incorporation into FeS₂ pyrite and its influence on dissolution: A DFT study: *Geochimica et Cosmochimica Acta*, v. 71(3), v. 624–630, doi: 10.1016/j.gca.2006.09.021.
- Breuer, C., Pichler, T. 2013, Arsenic in marine hydrothermal fluids: *Chemical Geology*, v. 348, p. 2–14, doi: doi.org/10.1016/j.chemgeo.2012.10.044.
- Brockbank, C.I., Batley, G.E., and Low, G. K.-C. 1998, Photochemical decomposition of arsenic species in natural waters: *Environmental and Technology Letters* v. 9, p. 1361–1366.

- Budinoff, C.R., and Hollibaugh, J.T., 2008, Arsenite-dependent photoautotrophy by an *Ectothiorhodospira*-dominated consortium: ISME Journal, v. 2, p. 340–343, doi: 10.1038/ismej.2007.115.
- Canfield, D.E., Ngombi-Pemba, L., Hammarlund, E.U., Bengtson, S., Chaussidon, M., Gauthier-Lafaye-Gauthier, F., Meunier, A., Riboulleau, A., Rollion-Bard, C., Rouxel, O., Asael, D., Pierson-Wickmann, A.-C., El Albani, A. 2013, Oxygen dynamics in the aftermath of the great oxidation of Earth's atmosphere: Proceedings of the National of Sciences U.S.A., v. 110(42), p. 16736–16741, doi: 10.1073/pnas.1315570110.
- Casentini, B., Pettine, M., and Millero, F., 2010, Release of arsenic from volcanic rocks through Interactions with inorganic anions and organic ligands: Aquatic Geochemistry, v. 16 (3), p. 373-393.
- Chen, J., Yoshinaga, M., Garbinski, L.D. and Rosen, B.P. 2016, Synergistic interaction of glyceraldehydes-3-phosphate dehydrogenase and ArsJ, a novel organoarsenical efflux permease, confers arsenate resistance: Molecular Microbiology, v. 100(6), p. 945-953, doi:10.1111/mmi.13371.
- Chen, J., Yoshinaga, M., and Rosen, B.P. 2018, antibiotic action of methylarsenite is an emergent property of microbial communities: Molecular microbiology, In Press, doi.org/10.1111/mmi.14169.
- Chen, S.-C., Sun, G.X., Rosen, B.P., Zhang, S.-Y., Deng, Y., Zhu, B.-K., Rensing, C., and Zhu, Y.-G. 2017, Recurrent horizontal transfer of arsenite methyltransferase genes facilitated adaptation of life to arsenic: Scientific Reports, v. 7(7741), <https://doi.org/10.1038/s41598-017-08313-2>.
- Chi Fru, E., Arvestål, E., Callac, N., El Albani, A., Kiliyas, S., Argyraki, A., and Jakobsson, M. 2015, Arsenic stress after the Proterozoic glaciations: Scientific Reports, v. 5(17789), doi:10.1038/srep17789.
- Chi Fru, E., Hemmingsson, C., Holm, M., and Iñiguez, E. 2016a, Arsenic-induced phosphate limitation under experimental Early Proterozoic oceanic conditions: Earth and Planetary Science Letters, v. 434, p. 52–63 doi:10.1016/j.epsl.2015.11.009.
- Chi Fru, E., Rodriguez, N.P., Partin, C.A., Lalonde, S.V., Andersson, P., Weiss, D.J., El Albani, A., Rodushkin, I., and Konhauser, K.O. 2016b, Cu isotopes in marine black shales record the Great Oxidation Event: Proceedings of the National Academy of Sciences, U.S.A.: v. 113(18), p. 4941–4946 doi:10.1073/pnas.1523544113.
- Chi Fru, E., Callac, N., Posth, N.R., Argyraki, A., Ling, Y.C., Ivarsson, M., Broman, C., and Kiliyas, S.P. 2018. Arsenic and high affinity phosphate uptake gene distribution in shallow submarine hydrothermal sediments: Biogeochemistry, v. 141(1), p. 41–46, doi.10.1007/s10533-018-0500-8(0123456789).
- Compton, J., Mallinson, D., Glenn, C.R., Filippelli, G., Föllmi, K., Shields, G., and Zanin, Y. 2000, Variations in the global phosphorus cycle: SEPM Special Publication, v. 66, p. 21–33.
- Couture, R.-M., Rose, J., Kumar, N., Mitchell, K., Wallschläger, D., and Van Cappellen, P. Sorption of arsenite, arsenate, and thioarsenates to iron oxides and iron sulfides: A kinetic and spectroscopic investigation: Environmental Science Technology, v. 47(11), p. 5652–5659, doi: 10.1021/es3049724.
- Craw, D., Falconer, D., and Youngson, J.H. 2003, Environmental arsenopyrite stability and dissolution: theory, experiment, and field observations: Chemical Geology, v. 199(1-2), p. 1–55.

- Cullen, W.R., Reimer, K.J. 1989, Arsenic speciation in the environment: Chemical Reviews, 89, 713-764, doi:10.1021/cr00094a002.
- de Sena Ferreira, G.R. 20016, Arsenic Mobilization from Silicic Volcanic Rocks in the Southern Willamette Valley. MSc. Thesis in Geology. Portland State University,
<file:///Users/CFernest/Desktop/Arsenic%20in%20volcanic%20rocks/37776136.pdf>.
- Dutta, P.K., Pehkonen, S.O., Sharma, V.K., and Ray, A.K. 2005, Photocatalytic oxidation of arsenic(III): Evidence of hydroxyl radicals: Environmental Science and Technology, v. 39(6), p. 1827–1834, doi:10.1021/es0489238.
- Dyhrman, S.T., and Haley, S.T. 2011, Arsenate resistance in the unicellular marine diazotroph *Crocospaera watsonii*: Frontiers Microbiology, <https://doi.org/10.3389/fmicb.2011.00214>.
- El Albani, A Bengtson, S., Canfield, D.E., Bekker, A., Macchiarelli, R., Mazurier, A., Hammarlund, E.U., Boulvais, P., Dupuy, J.-J., Fontaine, C., Fürsich, F.T., Gauthier-Lafaye, F., Janvierm P., Javaux, E., Ossa, F.O., Pierson-Wickmann, A.-C., Riboulleau, A., Sardini, P., Vachard, D., Whitehouse, M., and Meunier, A. 2010, Large colonial organisms with coordinated growth in oxygenated environments 2.1 billion years ago: Nature, v. 466, p. 100-104, doi:10.1038/nature09166.
- El Albani, A., Bengtson, S., Canfield, D.E., Riboulleau, A., Bard, C.R., Macchiarelli, R., Ngombi Pemba, L., Hammarlund, E., Meunier, A., Mouele, I.M., Benzerara, K., Bernard, S., Boulvais, P., Chaussidon, M., Cesari, C., Fontaine, C., Chi-Fru, E., Ruiz, J.M.G., Gauthier-Lafaye, F., Mazurier, A., Pierson-Wickmann, A.-C., Rouxel, O., Trentesaux, A., Vecoli, M., Versteegh, G.J.M., White, L., Whitehouse, M., and Bekker, A. 2014, The 2.1 Ga Old Francevillian Biota: Biogenicity, Taphonomy and Biodiversity: PLOS ONE, v. 9(6), e99438, doi:10.1371/journal.pone.0099438.
- Elias, M., Wellner, A., Goldin-Azulay, K., Chabriere, E., Vorholt, J.A., Erb, T.J., and Tawfik, D.S. 2012, The molecular basis of phosphate discrimination in arsenate-rich environments: Nature, v. 491(7422), p. 134–137.
- Emett, M.T., and Khoe, G.H. 2001, Photochemical oxidation of arsenic by oxygen and iron in acidic solutions: Water Research, v. 35(3), p 649–656, [https://doi.org/10.1016/S0043-1354\(00\)00294-3](https://doi.org/10.1016/S0043-1354(00)00294-3).
- Feely, R.A., Trefry, J.H., Massoth, G.J., and Metz, S. 1991. A comparison of the scavenging of phosphorus and arsenic from seawater by hydrothermal iron oxyhydroxides in the Atlantic and Pacific Oceans: Deep Sea Research Part A. Oceanographic Research Papers: v. 38(6), p. 617–623, doi:10.1016/0198-0149(91)90001-V.
- Fleet, M.E., and Mumin, A.H. 1997, Gold-bearing arsenian pyrite and marcasite and arsenopyrite from Carlin Trend gold deposits and laboratory synthesis: American Mineralogist, v. 82, p. 182–193, doi: 10.2138/am-1997-1-220.
- Foster, A.L. 2003, Spectroscopic investigation of arsenic species in solid phases. In Arsenic ground water (eds Welch, A.H. and Stollenwerk, K.G), Kluwer Academic Publishers, Boston, M.A., p. 27–65.
- Foster, A.L., and Kimm, C.S. 2014, Arsenic speciation in solids using X-ray absorption spectroscopy: Reviews in Mineralogy and Geochemistry, v. 79(1), p. 257-369, doi:10.2138/rmg.2014.79.5.

- Garellick, H., Jones, H., Dybowska, A., and Valsami-Jones, E. 2008, Arsenic pollution sources: Reviews of Environmental Contamination and Toxicology, v. 197, p. 17-60.
- Ghosh, M., Shen, J., and Rosen, B.P. 1999, Pathways of As(III) detoxification in *Saccharomyces cerevisiae*: Proceedings of the National Academy of Sciences of the United States of America, v. 96(9), p. 5001-5006, doi: doi.org/10.1073/pnas.96.9.5001.
- Gihring, T.M., Bond, P.L., Peters, S.C., and Banfield, J.F. 2003, Arsenic resistance in the archaeon "*Ferroplasma acidarmanus*": new insights into the structure and evolution of the ars genes: Extremophiles, v. 7(2), p. 123–130.
- Godelitsas, A., Price R.E., Pichler, T., Amend, J., Gamaletsos, P., and Göttlicher, J. 2015, Amorphous As-sulfide precipitates from the shallow-water hydrothermal vents off Milos Island (Greece): Marine Chemistry, v. 177, p. 687–696, doi. 10.1016/j.marchem.2015.09.004.
- Guidry, M.W., and Mackenzie, F.T. 2000, Apatite weathering and the Phanerozoic phosphate cycle: Geology, v. 28(7), p. 631–634, doi: 0.1130/0091-7613(2000)028<0631:AWATPP>2.3.CO;2.
- Gupta, S.K., and Chen, KY. 1978, Arsenic removal by adsorption: Journal of Water pollution Control Federation, v. 40, p. 493–506.
- Hao, X., Li, X., Pal, C., Larsson, D.G., Saquib, Q., Alwathnani, H.A., Rosen, B.P., Zhu, Y.G. and Rensing, C. 2017, Bacterial resistance to arsenic protects against arsenite killing: Biometals, v. 30(2), p. 307-311, doi:10.1007/s10534-017-0003-4.
- Hemmingsson, C., Pitcain, I., and Chi Fru, E. 2018, Evaluation of uptake mechanisms of phosphate by Fe(III)(oxyhydr)oxides in early Proterozoic oceanic conditions: Environmental Chemistry, v. 15(2), p. 18–28, <https://doi.org/10.1071/EN17124>.
- Henke, K.V. 2009, Arsenic: Environmental chemistry, health threats and waste treatment: Wiley, West Sussex, UK.
- Hoffmann, T., Warmbold, B., Smits, S.H.J., Tschapek, B., Ronzheimer, S., Bashir, A., Chen, C., Rolbetzki, A., Pittelkow, M., Jebbar, M., Seubert, A., Schmitt, L., and Bremer, E. 2018, Arsenobetaine: an ecophysiological important organoarsenical confers cytoprotection against osmotic stress and growth temperature extremes; Environmental Microbiology, v. 20(1), p. 305–323, doi: 10.1111/1462-2920.13999.
- Hug, S.J., Canonica, L., Wegelin, M., Gechter, D., and von Gunten, U. 2001, Solar oxidation and removal of arsenic at circumneutral pH in iron containing waters: Environmental Science and Technology, v. 35(10), p. 2114–2121, doi:10.1021/es001551s.
- Hug, S.J., and Leupin, O. 2003, Iron-catalyzed oxidation of arsenic(III) by oxygen and by hydrogen peroxide: pH-dependent formation of oxidants in the Fenton reaction: Environmental Science and Technology, v. 37(12), p. 2734–2742, doi:10.1021/es026208x.
- Jackson, C.R., Dugas, S.L. 2003, Phylogenetic analysis of bacterial and archaeal *arsC* gene sequences suggests an ancient, common origin for arsenate reductase: BMC Evolutionary Biology, <https://doi.org/10.1186/1471-2148-3-18>.
- Kasting, J.F., and Donahue, T.M. 1980, The evolution of atmospheric ozone: Journal of Geophysical Research, v. 85(C6), p. 3255–3263.

- Kendall, B., Reinhard, C.T., Lyons, T.W., Kaufman, A.J., Poulton, S.W., Anbar, A.D. 2010, Pervasive oxygenation along late Archean ocean margins: *Nature Geoscience*, v. 3, p. 647–652.
- Konhauser, K.O., Pecoits, E., Lalonde, S.V., Papineau, D., Nisbet, E.G., Barley, M.E., Arndt, N.T., Zahnle, K., and Kamber, B.S., 2009, Oceanic nickel depletion and a methanogen famine before the Great Oxidation Event: *Astrobiology*, v. 458(7239), p. 750–753.
- Konhauser, K.O., Lalonde, S.V., Planavsky, N.J., Pecoits, E., Lyons, T.W., Mojzsis, S.J., Rouxel, O.J., Barley, M.E., Rosière, C.A., Fralick, P.W., Kump, L.R., and Bekker, A., 2011, Aerobic pyrite oxidation and acid rock drainage during the Great Oxidation Event: *Nature*, v. 478, p. 369–374, doi:10.1038/nature10511.
- Kulp, T.R., Hoefft, S.E., Asao, M., Madigan, M.T., Hollibaugh, J.T., Fisher, J.C., Stolz, J.F., Culbertson, C.W., Miller, L.G., Oremland, R.S. 2008, Arsenic(III) fuels anoxygenic photosynthesis in hot spring biofilms from Mono Lake, California: *Science*, V. 15;321(5891), p. 967–70, doi: 10.1126/science.1160799.
- Lyons, T.W., Reinhard, C.T., and Planavsky, N.J., 2014, The rise of oxygen in Earth's early ocean and atmosphere: *Nature*, v. 506, p. 307–315, doi: 10.1038/nature13068.
- Martin, W., Baross, J., Kelley, D., and Russel, M.J. 2008, Hydrothermal vents and the origin of life: *Nature Reviews Microbiology*, v. 6(11), p. 805–814.
- McCann, S.H., Boren, A., Hernandez-Maldonado, J., Stoneburner, B., Saltikov, C.W., Stolz, J.F., and Oremland, R.S., 2017, Arsenite as an electron donor for anoxygenic photosynthesis: description of three strains of *Ectothiorhodospira* from mono lake, California and Big Soda Lake, Nevada: *Life*, v. 7(1), doi: 10.3390/life7010001.
- McLennan, S.M. 2001, Relationships between the trace element composition of sedimentary rocks and upper continental crust: *Geochemistry, Geophysics, Geosystems*, v. 2(4), doi: 10.1029/2000GC000109.
- Meharg, A.A., and Hartley-Whitaker, J., 1999, Arsenic uptake mechanism in arsenic resistant and nonresistant plant species: *New Phytologist*, 154, 29–43, doi.org/10.1046/j.1469-8137.2002.00363.x.
- Mulkidjanian, A.Y., Bychkov, Y.A., Dibrova, V., Galperin, M.Y., Koonin, E.V., 2012. Origin of first cells at terrestrial, anoxic geothermal fields: *Proceedings of the National Academy of the United States of America*, v. 109 (14), p. E821–E830, <https://doi.org/10.1073/pnas.1117774109>.
- Muntean, J.L., Cline, J.S., Simon, A.C., and Longo, A.A., 2011, Magmatic-hydrothermal origin of Nevada's Carlin-type gold deposits: *Nature Geosciences*, v. 4, p. 122–127.
- Neppolian, B., Celik, E., and Choi, H. 2008, Photochemical oxidation of arsenic(III) to arsenic(V) using peroxydisulfate ions as an oxidizing agent: *Environmental Science and Technology*, v. 42(16), p. 6179–6184, doi: 10.1021/es800180f.
- Nesbitt, H.W., Muir, I.J., and Pratt, A.R. 1995, Oxidation of arsenopyrite by air and air-saturated, distilled water, and implications for mechanism of oxidation: *Geochemica et Cosmochimica Acta*, v. 59(9), p. 1773–1786.

- Ngombi-Pemba, L., El Albani, A., Meunier, A., Grauby, O., and Gauthier-Lafaye, F. 2014, From detrital heritage to diagenetic transformations, the message of clay minerals contained within shales of the Palaeoproterozoic Francevillian basin (Gabon): *Precambrian Research*, v. 255, p. 63–76, doi:10.1016/j.precamres.2014.09.016.
- Nordstrom, D.K., and Archer, D.G. 2003, Arsenic thermodynamic data and environmental geochemistry. In *Arsenic in ground water* (eds Welch, A.H., and Stollenwerk, K.G.). Kluwer Academic Publishers, Boston, MA, p.1–25.
- O'Day, P.A., Vlassopoulos, D., Root, R., and Rivera, N. 2004, The influence of sulfur and iron on dissolved arsenic concentrations in the shallow subsurface under changing redox conditions: *Proceedings of the National Academy of Sciences, U.S.A.*, v. 101, p. 13703–13708, doi:10.1073/pnas.0402775101.
- O'Day, P.A. 2006, *Chemistry and mineralogy of arsenic: Elements*, v. 2, p. 77–83.
- Oremland, R.S., Hoefft, S.E., Santini, J.M., Bano, N., Holobaugh, R.A., and Hollibaugh, J.T., 2002, Anaerobic oxidation of arsenite in Mono Lake water and by a facultative, arsenite-oxidizing chemoautotroph, strain MLHE-1: *Applied and Environmental Microbiology*, v. 68(10), p. 4795–4802.
- Oremland, R.S., and Stolz, J.F. 2003, The ecology of arsenic: *Science*, v. 300(5621), p. 939–944, doi: 10.1126/science.1081903.
- Planavsky, N.J., Bekker, A., Hofmann, A., Owens, J.D., and Lyons, T. W. 2012, Sulfur record of rising and falling marine oxygen and sulfate levels during the lomagundi event: *Proceedings of the National Academy of Science U.S.A.*, v. 109, p. 18300–18305.
- Poulton, S.W., and Canfield, D.E. 2011, Ferruginous conditions: A dominant feature of the ocean through Earth's history: *Elements*, v 7(2), p. 107–112, doi:10.2113/gselements.7.2.107.
- Price, R.E., Savov, I., Planer-Friedrich, B., Bühring, S.I., Amend, J., and Pichler, T., 2013, Processes influencing extreme As enrichment in shallow-sea hydrothermal fluids of Milos Island, Greece: *Chemical Geology*, v. 348, p. 15–16, doi:10.1016/j.chemgeo.2012.06.007.
- Qin, J., Rosen, B.P., Zhang, Y., Wang, G., Franke, S., and Rensing, C. 2006, Arsenic detoxification and evolution of trimethylarsine gas by a microbial arsenite S-adenosylmethionine methyltransferase: *Proceedings of the National Academy of Sciences of the United States of America*, v. 103 (7), p. 2075–2080, doi. 10.1073/pnas.0506836103.
- Qin, J., Fu, H.-L., Ye, J., Bencze, K.Z., Stemmler, T.L., Rawlings, D.E., Rosen, B.P. 2007. Convergent Evolution of a New Arsenic Binding Site in the ArsR/SmtB Family of Metalloregulators: *Journal of Biological Chemistry*, v. 282(47), p. 34346–34355, doi: 10.1074/jbc.M706565200.
- Reinhard, C.T., Planavsky, N.J., Robbins, L.J., Partin, C.A., Gill, B.C., Lalonde, S.V., Bekker, A., Konhauser, K.O., and Lyons, T.W. 2013, Proterozoic ocean redox and biogeochemical stasis: *Proceedings of the National Academy of Sciences U.S.A.*, v. 110 (14), p. 5357–5362; <https://doi.org/10.1073/pnas.1208622110>.
- Reynaud, J.-Y., Trentesaux, A., El Albani, A., Aubineau, J., Ngombi-Pemba, L., Guiyeligou, G., Bouton, P., Gauthier-Lafaye, F., and Weber, F. 2017, Depositional setting of the 2.1 Ga Francevillian macrobiota (Gabon): *Rapid*

- mud settling in a shallow basin swept by high-density sand glows: *Sedimentology*: In Press, doi:10.1111/sed.12398.
- Robbins, L.J., Lalonde, S.V., Saito, M.A., Planavsky, N.J., Mloszewska, A., Pecoits, E., Scott, C., Dupont, C.L., Kappler, A., and Konhauser, K.O. 2013, Authigenic iron oxide proxies for marine zinc over geological time and implications for eukaryotic metallome evolution: *Geobiology*, v. 11(4), p. 295–306, doi: 10.1111/gbi.12036.
- Rothstein, A. 1963, Interactions of arsenate with the phosphate-transporting system of yeast: *Journal of General Physiology*, v. 46, p. 1075–1085, doi: 10.1085/jgp.46.5.1075.
- Samantha, L.S., Singireddy, S., Thenuwara, A.C., Attanayake, N.H., Reeder, R.J., and Strogan, D.R. 2016, Oxidation of arsenite to arsenate on birnessite in the presence of light: *Geochemical Transactions*, v. 17(5), doi: 10.1186/s12932-016-0037-5.
- Savoie, C.B.Y. 2013, Arsenic Mobility and Compositional Variability in High-Silica Ash Flow Tuffs: MSc. Thesis in Geology, Portland State University, https://pdxscholar.library.pdx.edu/cgi/viewcontent.cgi?article=2011&context=open_access_etds.
- Schaufuss, A.G., Nesbitt, H.W., Scaini, M.J. et al. 2000, Reactivity of surface sites on fractured arsenopyrite (FeAsS) toward oxygen: *American Mineralogist*, v. 85(11-12), p. 1754–1766.
- Scott, C., Wing, B.A., Bekker, A., Planavsky, N.J., Medvedev, P., Bates, S.M., Yun, M., and Lyons, T.W. 2014, Pyrite multiple-sulfur isotope evidence for rapid expansion and contraction of the early Paleoproterozoic seawater sulfate reservoir: *Earth and Planetary Science Letters*, v. 389, p. 95–104, doi:10.1016/j.epsl.2013.12.010.
- Schröder, S., Bedorf, D., and Gutzmer, J. 2011, From BIF to red beds: Sedimentology and sequence stratigraphy of the Paleoproterozoic Koegas Subgroup (South Africa): *Sedimentary Geology*, v. 236 (1-2), p. 25–44, doi: 10.1016/j.sedgeo.2010.11.007.
- Sforna, M.C., Philippot, P., Somogyi, A., van Zuilen, M.A., Medjoubi, K., Schoepp-Cathenet, B., Nitschke, W., and Visscher, P.T. 2014, Evidence for arsenic metabolism and cycling by microorganisms 2.7 billion years ago: *Nature Geoscience*, v. 7, p. 811–815, doi:10.1038/ngeo2276.
- Silver, S., and Phung, L.T. 2005, Genes and enzyme involved in bacterial oxidation and reduction of inorganic arsenic: *Applied & Environmental Microbiology*, v. 71(2), p. 599–608, doi:10.1128/AEM.71.2.599-608.2005.
- Smedley, P.L., and Kinniburgh, D.G. 2002, A review of the source, behaviour and distribution of arsenic in natural waters: *Applied Geochemistry*, v 17(5), p. 517–568, doi:10.1016/S0883-2927(02)00018-5.
- Solé, V.A., Papillon, E., Cotte, M., Walter, P., Susini, J. 2005. A multiplatform code for the analysis of energy-dispersive X-ray fluorescence spectra: *Spectrochimica Acta Part B*, v. 62, p. 63-68.
- Somogyi, A., Medjoubi, K., Baranton, G., Roux, L., Ribbens, M., Polack, F., Philippot, P., and Samama, J.P. 2015, Optical design and multi-length-scale scanning spectro-microscopy possibilities at the Nanoscopium beamline of Synchrotron Soleil: *Journal of Synchrotron Radiation*, v. 22(4), p. 1118–1129, doi:10.1107/S1600577515009364.

- Swanwoth, C.W., and Badham, J.P.N. 1984, Lower Proterozoic red beds, evaporites and secondary sedimentary uranium deposits from the East Arm, Great Slave Lake, Canada: *Journal of the Geological Society*, v. 141, p. 235–242, doi: 10.1144/gsjgs.141.2.0235.
- Tian, X., and Luo, K. 2017, Selenium, arsenic and molybdenum variation and bio-radiation in the Ediacaran-Cambrian interval: *Precambrian Research*, v. 292, p. 378–385, doi:10.1016/j.precamres.2017.02.007.
- Thiel, T. 1988, Phosphate transport and arsenate resistance in the cyanobacterium *Anabaeba variabilis*: *Journal of Bacteriology*, v. 170(3), p. 1143–1147, doi:10.1128/jb.170.3.1143-1147.1988.
- Toumassat, C., Charlet, C., Bosbach, D., and Manceau, A. 2002, Arsenic(III) oxidation by birnessite and precipitation of manganese(II) arsenate: *Environmental Science Technology*, v. 36(3), p. 493–500, doi: 10.1021/es0109500.
- Vaughan, D.J., and Corkhill, C.L. 2017, Minerology of sulfides: *Elements*, v. 13, p. 81–87, doi: 10.2113/gselements.13.2.81.
- Vorliceck, T.P., Helz, G.R., Chappaz, A., Vue, P., Vezina, A., Hunter, W. 2018, Molybdenum burial mechanism in sulfidic sediments; iron-sulfide pathway: *ACS Earth Space Chemistry*, v. 2 (6), p. 565–576.
- Walker, J.C.G. 1977, The early history of oxygen and ozone in the atmosphere: *Pure and Applied Geophysics*, v. 117(3), p. 498–512.
- Welch, A.H., Westjohn, D.B., Helsel, D.R., and Wanty, R.B. 2000, Arsenic in ground water of the united states: occurrence and geochemistry: *Ground Water*, v. 38(4), p. 589–604.
- Webster, J.G., Nordstrom, K., 2003, Geothermal arsenic. In: Welch, A., Stollenwerk, K., eds., *Arsenic in Ground Water*, Kluwer Academic Publishers, New York, Boston, Dordrecht, London, Moscow, pp. 101–126.
- Williams, M. 2001, Arsenic in mine waters: international study: *Environmental Geology*: v. 40(3), p. 267–278.
- Yang, K., and Scott, S.D. 1996, Possible contribution of a metal-rich magmatic fluid to a seafloor hydrothermal system: *Nature*, v. 383(3), p. 420–423.
- Ye, J., Rensing, C., Rosen, B.P., and Zhu, Y.G., 2012, Arsenic biomethylation by photosynthetic organisms: *Trends in Plant Sciences*, v. 17(3), p. 155– 162, doi:10.1016/j.tplants.2011.12.003.
- Zerkle, AL., Poulton, S.W., Newton, R.J., Mettam, C., Claire, M.W., Bekker, A., and Junium, C.K. 2017, Onset of the aerobic nitrogen cycle after the Great Oxidation Event: *Nature*, v. 542, p. 465–467, doi:10.1038/nature20826.
- Zhang, J., Zhao, S., Xu, Y., Zhou, W., Huang, K., Tang, Z., Zhao, F-J., 2017, Nitrate stimulates anaerobic microbial arsenite oxidation in paddy soils: *Environmental Science Technology*, v. 51, p. 4377–4386, doi: 10.1021/acs.est.6b062.

Table S1. X-ray absorption near edge spectroscopy (XANES) data and total As concentration determined by X-ray fluorescence (XRF), for shale samples from the Transvaal Supergroup in South Africa, the Francevillian series in Gabon and the Zaonega formation in Russia. A 15% XANES detection limit implies that a given As species could only be decomposed from the XANES spectrum if it was >15% of the total As concentration.

Sample	Lithology	Formation	Location	Depth (m)	Age (Ga)	Total As (ppm)	Arsenate (%)	Arsenite (%)	Arsenic sulfides (%)
12B	Black shale	Zaonega	Fennoscandian	133.18	1.98	235	34	<15	60
12B	Black shale	Zaonega	Fennoscandian	212.9	1.98	45	<15	<15	100
12B	Black shale	Zaonega	Fennoscandian	251.98	1.98	47	46	<15	39
B16	Black shale	FD	Franceville	6.5	2.083	210	<15	<15	86
B9	Black shale	FD	Franceville	6.5	2.083	140	22	<15	77
LEK	Black shale	FB	Franceville	16.7	2.1	<1	<15	<15	<15
SOC F1	Black shale	FB	Franceville	17.5	2.1	<1	<15	<15	<15
SOC F2	Black shale	FB	Franceville	18.8	2.1	<1	<15	<15	<15
SOC F3	Black shale	FB	Franceville	19.2	2.1	<1	<15	<15	<15
SOC F4	Black shale	FB	Franceville	19.7	2.1	<1	<15	<15	<15
KO 42028	Black shale	FB	Franceville	80.95	2.1	870	55	19	25
KO 42028	Black shale	FB	Franceville	96.5	2.1	30	24	<15	73
KO 42028	Black shale	FB	Franceville	110.2	2.1	70	20	<15	78
TF1/72	Black shale	Timeball Hill	Transvaal	240	2.32	4	<15)	<15	84
TF1/72	Black shale	Timeball Hill	Transvaal	240	2.32	4	<15	<15	88
TF1/72	Black shale	Timeball Hill	Transvaal	240	2.32	4	17	<15	78
TF1/72	Black shale	Timeball Hill	Transvaal	360	2.32	60	42	<15	54
TF1/72	Black shale	Timeball Hill	Transvaal	360	2.32	60	37	<15	65
TF1/72	Black shale	Timeball Hill	Transvaal	360	2.32	60	31	<15	63
TF1/72	Black shale	Timeball Hill	Transvaal	460	2.32	5	32	<15	69
TF1/72	Siliceous shale	Rooihoogte	Transvaal	578	2.34	<1	<15	<15	<15

TF1/72	Siliceous shale	Rooihoogte	Transvaal	580.2	2.34	<1	<15	<15	<15
TF1/72	Black shale	Eccles	Transvaal	590	2.45	1.5	<15	<15	<15
TF1/72	Black shale	Eccles	Transvaal	594.15	2.45	45	<15	<15	100
TF1/72	Dolomitic shale	Eccles	Transvaal	1066.5	2.48	0.6	47	<15	52
TF1/72	Dolomitic shale	Eccles	Transvaal	1066.5	2.48	0.6	45	<15	47
TF1/72	Black shale	Monte Cristo	Transvaal	580	2.5	<1	<15	<15	<15
TF1/72	Dolomitic shale	Lyttleton	Transvaal	1450	2.5	<1	<15	<15	<15
TF1/72	Dolomitic shale	Lyttleton	Transvaal	2800	2.5	<1	<15	<15	<15
TF1/72	Dolomitic shale	Oak Tree	Transvaal	2138.2	2.55	<1	<15	<15	<15
TF1/72	Dolomitic shale	Oak Tree	Transvaal	2200	2.6	<1	<15	<15	<15
TF1/72	Dolomitic shale	Oak Tree	Transvaal	2300	2.6	<1	<15	<15	<15
TF1/72	Dolomitic shale	Bothaville	Transvaal	2391.8	2.7	<1	<15	<15	<15
TF1/72	Dolomitic shale	Bothaville	Transvaal	2430.0	2.7	<1	<15	<15	<15
TF1/72	Dolomitic shale	Bothaville	Transvaal	2339.5	2.7	<1	<15	<15	<15
TF1/72	Dolomitic shale	Bothaville	Transvaal	2349.7	2.7	<1	<15	<15	<15
TF1/72	Dolomitic shale	Bothaville	Transvaal	2440	2.7	<1	<15	<15	<15
TF1/72	Dolomitic shale	Bothaville	Transvaal	2450	2.7	<1	<15	<15	<15
TF1/72	Dolomitic shale	Bothaville	Transvaal	2452.5	2.714	<1	<15	<15	<15

Table DR2

2019089 Table DR2.xlsx